

Ab initio quasi-harmonic thermoelasticity of molybdenum at high temperature and pressure

X. Gong^{1,2} and A. Dal Corso^{1,2}

¹*International School for Advanced Studies (SISSA), Via Bonomea 265, 34136, Trieste, Italy*

²*IOM - CNR, Via Bonomea 265, 34136, Trieste, Italy*

(*Electronic mail: xgong@sisssa.it)

(Dated: 25 June 2024)

We present the ab-initio thermoelastic properties of body-centered cubic molybdenum under extreme conditions obtained within the quasi-harmonic approximation including both the vibrational and the electronic thermal excitations contributions to the free energy. The quasi-harmonic temperature dependent elastic constants are calculated and compared with existing experiments and with the quasi-static approximation. We find that the quasi-harmonic approximation allows a much better interpretation of the experimental data confirming the trend found previously in other metals. Using the Voigt-Reuss-Hill average we predict the compressional and shear sound velocities of polycrystalline molybdenum as a function of pressure for several temperatures which might be accessible in experiments.

I. INTRODUCTION

Molybdenum, as a refractory $4d$ transition metal in the same group of tungsten, finds several applications, pure or in alloys with other metals, for its high melting point, mechanical properties, and corrosion resistance. Its thermodynamic properties have been studied by several authors, both experimentally and by theory.¹⁻¹³

Among the thermodynamic properties, the elastic constants (ECs) are key parameters that determine the mechanical stability, the velocity of sound waves, and the stress response to external strains. In this regard, particularly useful for applications is the pressure and temperature dependence of the ECs. In molybdenum, the temperature dependent bulk modulus and ECs have been measured by ultrasonic technique at room pressure.¹⁴⁻¹⁷ Data are available almost until melting (2898 K).¹⁷ Pressure derivatives of the ECs are known at room temperature¹⁸ and compressional and shear sound velocities in polycrystalline molybdenum have been measured up to 120 kbar at room temperature.¹⁹ A simultaneous measurement of the density allow to derive from these data the bulk and shear moduli at high pressure. However, information on pressure dependent elasticity at high temperatures is still missing in the literature.

Theoretically temperature dependent ECs of molybdenum have been calculated within the quasi-static approximation (QSA) at room pressure,²⁰ while the pressure dependent ECs have been calculated by Koči et al.²¹ at zero temperature. The measurements on polycrystalline molybdenum have been modeled by ab-initio calculations¹⁹ and the ECs along the Hugoniot together with the corresponding compressional and shear sound velocities have been calculated within the QSA.¹⁰ Due to the time-consuming phonon calculations for deformed configurations of metallic systems needed for the ab-initio quasi-harmonic (QHA) ECs no paper has addressed these quantities for molybdenum so far.

In recent years, a workflow for the calculation of the QHA ECs within density functional theory (DFT) has been fully integrated in the `thermo_pw` software,^{22,23} continuously im-

proved, and applied to several solids (aluminum, silicon, BAs, copper, silver, gold, palladium, platinum, and tungsten).²⁴⁻²⁷ In many metals, it has been found that the QHA predicts the temperature dependence of the ECs accurately, much more than the QSA.^{23,28} The 0 K values instead are similar and might differ from experiment, with differences that depend on the exchange and correlation functional and are usually within 10 %.

In this paper we apply this technique to molybdenum. We present a comparison of the temperature dependence of the QSA and the QHA ECs and use the calculated QHA adiabatic ECs to predict the temperature and pressure dependence of the bulk and shear moduli of polycrystalline molybdenum as well as its compressional and shear sound velocities, providing a theoretical prediction that could be useful in future investigations of the thermoelastic properties at high pressure and temperature.

II. THEORY AND COMPUTATIONAL PARAMETERS

Within the QHA, the Helmholtz free energy of a cubic solid is a function of temperature T and (unit cell) volume V . It can be written as the sum of three contributions:

$$F(V, T) = U(V) + F_{ph}(V, T) + F_{el}(V, T), \quad (1)$$

where $U(V)$ is the static energy, computed by DFT, $F_{el}(V, T)$ is the electronic thermal excitations contribution to the free energy, and $F_{ph}(V, T)$ is the vibrational free energy written in terms of the phonon frequencies $\omega_\eta(\mathbf{q}, V)$:

$$F_{vib}(V, T) = \frac{1}{2N} \sum_{\mathbf{q}\eta} \hbar \omega_\eta(\mathbf{q}, V) + \frac{1}{N\beta} \sum_{\mathbf{q}\eta} \ln [1 - \exp(-\beta \hbar \omega_\eta(\mathbf{q}, V))]. \quad (2)$$

N is the total number of cells in the solid (equal to the number of \mathbf{q} vectors in the sum) and \hbar is the reduced Planck's constant.

TABLE I. The equilibrium lattice constants (a_0), the bulk moduli (B_T) and the pressure derivatives of the bulk moduli (B'_T) of molybdenum calculated in this work compared with previous calculations and with experiment.

		T	a_0	B_T	B'_T
		(K)	(a.u.)	(kbar)	
This study	LDA	0	5.884	2949	4.00
		295	5.894	2874	4.09
	PBEsol	0	5.916	2826	4.02
		295	5.926	2753	4.10
	PBE	0	5.975	2617	4.08
		295	5.986	2543	4.16
Calc. ⁹	PW91	0	5.988	2666	4.42
Calc. ¹⁰	PBE	0	5.996	2633	4.21
Calc. ²¹	PBE	0	6.001	2610	4.5
Calc. ^{12a}	PBE	0	5.992		
Calc. ²⁹	LDA	0	5.888		
	PBEsol	0	5.920		
	PBE	0	5.979		
Calc. ²	LDA	0	5.880	3010	3.99
		298 ^b	5.891	2950	4.01
	PBEsol	0	5.914	2870	4.02
		298 ^b	5.925	2800	4.05
	PBE	0	5.981	2620	4.14
		298 ^b	5.993	2550	4.17
Model ⁴		300	5.945	2600	4.21
Model ³⁰		300	5.944	2605	4.05
Expt. ^{2a}		300	5.944	2610	4.06
Expt. ¹		300	5.951	2608	4.46
Expt. ¹⁴		0		2653	
Expt. ³¹				2610	4.65 ^c /3.95 ^d

^a These data are used to calculate the equations of state which we report in Fig. S2 and Fig. S3 of the supplementary material.

^b Values estimated using a Debye model.

^c Ultrasonic experiment.

^d Shock Wave experiment.

\mathbf{q} are the phonon wave vectors and the subscript η indicates the different vibrational modes.

The contribution of the electronic thermal excitations to the free energy is calculated within the rigid bands approximation²⁶ as $F_{el} = U_{el} - TS_{el}$. U_{el} is electronic excitation contribution to the energy given by

$$U_{el} = \int_{-\infty}^{\infty} EN(E)f(E, T, \mu)dE - \int_{-\infty}^{E_F} EN(E)dE, \quad (3)$$

where E_F is the Fermi energy, $N(E)$ is the electronic density of states, $f(E, T, \mu)$ are the Fermi-Dirac occupations, μ is the chemical potential, and S_{el} is the electronic entropy given by:

$$S_{el} = -k_B \int_{-\infty}^{\infty} \left[f(E, T, \mu) \ln f(E, T, \mu) + (1 - f(E, T, \mu)) \ln(1 - f(E, T, \mu)) \right] N(E)dE. \quad (4)$$

For a certain number of geometries N_V , a fourth order Birch-Murnaghan equation is applied to interpolate the $U(V)$ at cell volumes V_i , $i = 1, 2, \dots, N_V$. The vibrational and electronic free energies are fitted at each temperature by a fourth degree polynomial as a functions of V . The computational details for the volume thermal expansion β_V , the isobaric heat capacity C_p , the isoentropic bulk modulus B_S and the average Grüneisen parameter are given in the supplementary material.

The isothermal ECs are calculated from the second strain derivatives of the free energy:

$$\tilde{C}_{ijkl}^T = \frac{1}{V} \left. \frac{\partial^2 F}{\partial \epsilon_{ij} \partial \epsilon_{kl}} \right|_T, \quad (5)$$

correcting for finite pressure effects to obtain the stress-strain ECs:³²

$$C_{ijkl}^T = \tilde{C}_{ijkl}^T + \frac{P}{2} (2\delta_{i,j}\delta_{k,l} - \delta_{i,l}\delta_{j,k} - \delta_{i,k}\delta_{j,l}). \quad (6)$$

The second derivatives of the free energy are calculated as described in Ref.²³ taking a subset of the volumes V_i as equilibrium configurations. The ECs at any other volume at temperature T and pressure p are obtained by interpolation by a fourth-degree polynomial. Adiabatic ECs are calculated from the isothermal ones as:

$$C_{ijkl}^S = C_{ijkl}^T + \frac{TVb_{ij}b_{kl}}{C_V}, \quad (7)$$

where b_{ij} are the thermal stresses:

$$b_{ij} = -\sum_{kl} C_{ijkl}^T \alpha_{kl}, \quad (8)$$

and C_V is the isochoric heat capacity (See the supplementary material). For a cubic system, the linear thermal expansion tensor is diagonal and from the volume thermal expansion β_V we get: $\alpha_{kl} = \delta_{kl}\beta_V/3$. With the knowledge of the adiabatic ECs, using the Voigt-Reuss-Hill approximation, we compute the polycrystalline average of the bulk modulus B_S , of the shear modulus G_S , of the Young's modulus E_S , and of the Poisson's ratio ν_S (see the thermo_pw manual for the expressions used). Finally, the compressional and the shear sound velocities are given by:

$$V_P = \sqrt{\frac{B_S + 4/3G_S}{\rho}}, \quad (9)$$

$$V_G = \sqrt{\frac{G_S}{\rho}}, \quad (10)$$

where ρ is the density. Note that these equations also hold with pressure as long as B_S and G_S are computed from the stress-strain ECs.³³

The temperature and pressure dependent thermodynamic properties and ECs are calculated by the open source software thermo_pw, which has been discussed in previous publications.^{23–27,34,35}

The calculations presented in this work are done by using DFT as implemented in the Quantum ESPRESSO (QE) package.^{36,37} The exchange and correlation functionals are the LDA³⁸ and the generalized gradient approximations PBEsol³⁹ and PBE.⁴⁰

We employ the projector augmented wave (PAW) method⁴¹ and a plane-wave basis with pseudopotentials from `pslibrary`.⁴² We use `Mo.pz-spn-kjpaw_psl.1.0.0.UPF`, `Mo.pbesol-spn-kjpaw_psl.1.0.0.UPF`, and `Mo.pbe-spn-kjpaw_psl.1.0.0.UPF` for LDA, PBEsol, and PBE, respectively. These pseudopotentials have the $4s$, $4p$, $4d$, and $5s$ states in the valence, while the other states are frozen in the core and accounted for by the nonlinear core correction.⁴³ The lattice constants of 14 reference geometries from 4.784 a.u. to 6.084 a.u. with LDA, from 4.8162 a.u. to 6.1162 a.u. for PBEsol, and from 4.8922 a.u. to 6.1922 a.u. with PBE with an interval of 0.1 a.u. between geometries have been chosen to calculate the free energies. For the wave functions cutoffs, we use 100 Ry, 90 Ry, 120 Ry while for the charge density we use 400 Ry, 360 Ry, 480 Ry, for LDA, PBEsol, and PBE, respectively. The Fermi surface has been dealt with by the smearing approach of Methfessel and Paxton⁴⁴ with a smearing parameter $\sigma = 0.02$ Ry. With this smearing, the Brillouin zone integrals converge with a $40 \times 40 \times 40$ \mathbf{k} -point mesh.

For 6 reference geometries (with $i = 1, 4, 7, 11, 12, 13$), temperature dependent ECs are calculated by 3 strain types that lead to a body-center cubic, a centered tetragonal, and a rhombohedral strained lattices. Each strain type is sampled by 6 strains, from $\varepsilon = -0.15$ to $\varepsilon = 0.15$ with stepsize $\delta\varepsilon = 0.05$. A thicker \mathbf{k} -point mesh of $45 \times 45 \times 45$ is employed on strained configurations. Each one of the 108 strained configurations requires calculations of phonon frequencies and electronic density of states. Phonon frequencies are calculated by density functional perturbation theory (DFPT)^{45,46} getting the dynamical matrices on a $8 \times 8 \times 8$ \mathbf{q} -point grid. These dynamical matrices have been Fourier interpolated on a $200 \times 200 \times 200$ \mathbf{q} -point mesh to evaluate the free-energy and the thermodynamic quantities. The calculations are all performed on the Leonardo supercomputer at CINECA with a GPU version of `thermo_pw` that optimizes some routines of QE for problems with dense \mathbf{k} -points sampling in metallic systems.⁴⁷

III. RESULTS AND DISCUSSION

In Table I, the equilibrium lattice constants, bulk moduli, and pressure derivatives of the bulk moduli of molybdenum obtained as parameters of a fourth-order Birch-Murnaghan interpolation of the static energy $U(V)$ are listed together with a few selected values from previous calculations and experiment. Our PAW LDA, PBEsol, and PBE values of the lattice constant differ by less than 0.1% from the all-electron values reported in Ref.²⁹. With respect to experiment ($a = 5.936$ a.u. at 0 K) the LDA, PBEsol, and PBE errors are -0.9% , -0.3% and 0.7% , with LDA and PBEsol below experiment and PBE above. For the bulk modulus these errors become 10% (LDA),

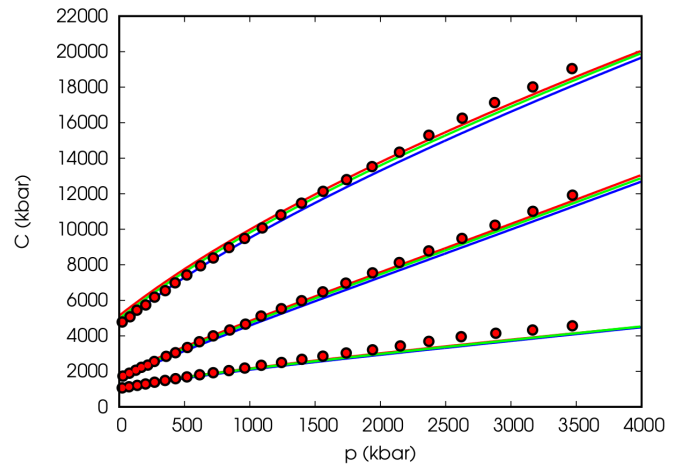


FIG. 1. Elastic constants as a function of pressure calculated within LDA (red lines), PBEsol (green lines) and PBE (blue lines) compared with the PBE results of Ref.²¹.

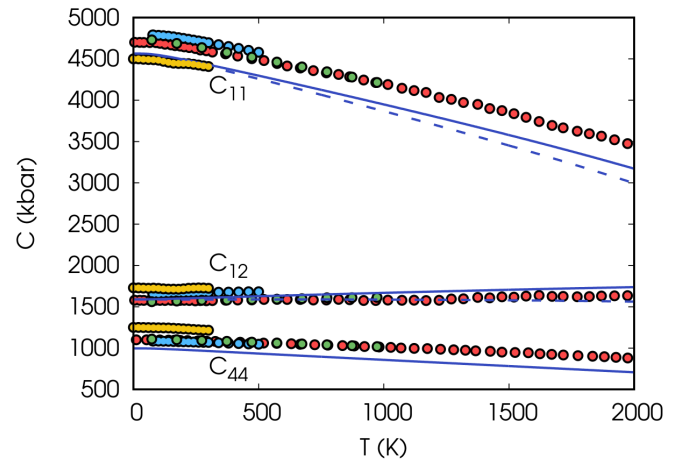


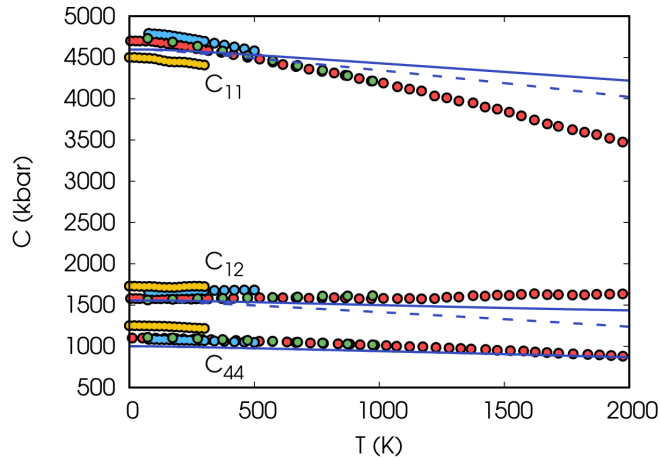
FIG. 2. Quasi-harmonic isothermal (dashed lines) and adiabatic (solid line) elastic constants C_{11} , C_{12} and C_{44} as a function of temperature compared with experimental adiabatic data from Ref.¹⁴ (yellow circles), Ref.¹⁶ (green circles), Ref.¹⁵ (blue circles), and Ref.¹⁷ (red circles).

7% (PBEsol), and -1% (PBE) with respect to the 0 K value 2653 kbar.¹⁴

In Table II, we report the values of the ECs C_{11} , C_{12} , and C_{44} calculated with the three functionals together with the values of the bulk modulus, Young's modulus, shear modulus, and Poisson's ratio of polycrystalline molybdenum calculated using the Voigt-Reuss-Hill approximation. The temperature dependent ECs have been measured in Refs.¹⁴⁻¹⁷. Although there is not perfect agreement among these data, the 0 K values of Ref.¹⁶⁻¹⁸ are quite close to each other. Taking as a reference the values of Ref.¹⁸ extrapolated to 0 K, by adding the theoretical difference between 0 K and 300 K, we find that the LDA errors for C_{11} , C_{12} , and C_{44} are 399 kbar (8%), 219 kbar (14%) and -27 kbar (-2%) while the PBE errors are -147 kbar (-3%), -7 kbar (-0.4%) and -105 kbar (-9

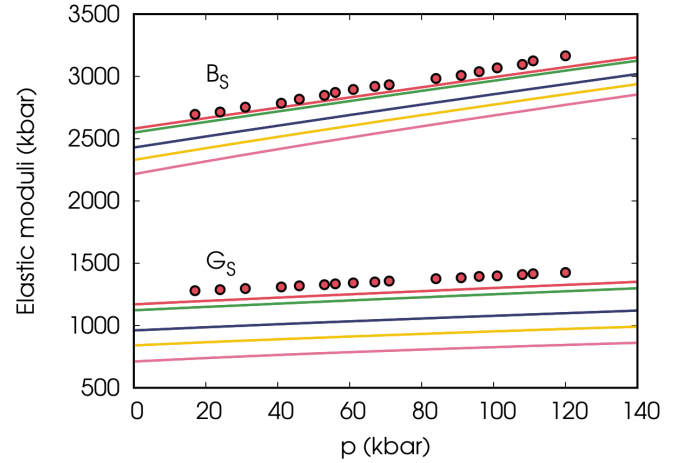
TABLE II. The 0 K elastic constants calculated with the different functionals compared with experiment and one previous calculation. B , E , G , and ν are the bulk modulus, the Young's modulus, the shear modulus, and the Poisson's ratio, respectively.

	T (K)	a_0 (a.u.)	C_{11} (kbar)	C_{12} (kbar)	C_{44} (kbar)	B (kbar)	E (kbar)	G (kbar)	ν
LDA	0	5.884	5183	1815	1094	2938	3402	1301	0.307
PBEsol	0	5.916	4976	1727	1081	2810	3318	1273	0.303
PBE	0	5.974	4637	1589	1016	2605	3111	1196	0.301
PW91 ⁹	0	5.988	4723	1604	1060	2644	3211	1237	0.297
Expt. ¹⁴	0		4500.2	1729.2	1250.3	2653	3358	1303	0.289
Expt. ¹⁶	273.15		4637	1578	1092	2598	3232	1250	0.293
Expt. ¹⁶ (Extrapolated)	0		4800	1558	1124	2639	3354	1302	0.288
Expt. ¹⁵	300		4696	1676	1068	2683	3194	1227	0.302
Expt. ¹⁵ (Extrapolated)	0		4832	1656	1100	2715	3306	1275	0.297
Expt. ¹⁸	300		4648	1616	1089	2627	3222	1244	0.296
Expt. ¹⁸ (Extrapolated)	0		4784	1596	1121	2659	3334	1291	0.291
Expt. ¹⁹	300					2607		1251	

FIG. 3. Quasi-static isothermal (dashed lines) and adiabatic (solid line) elastic constants C_{11} , C_{12} , and C_{44} as a function of temperature compared with adiabatic experimental data from Ref.¹⁴ (gold circles), Ref.¹⁶ (green circles), Ref.¹⁵ (blue circles), and Ref.¹⁷ (red circles).

%). PBEsol has errors 192 kbar (4 %), 131 kbar (8 %), and -40 kbar (-4 %) smaller than LDA, but bigger than PBE. The PBE values of C_{11} and C_{12} , and hence of its bulk modulus, are the closest to experiment. Since the calculation of the TDEC is computationally heavy, we calculated them using only this functional. Actually, as shown in Ref.²⁶ for several metals and as we confirmed in a recent study of tungsten,² different functionals give different 0 K values of the ECs but the temperature and pressure dependence is almost independent from the functional.

In Fig. 1 we present the pressure dependent ECs at 0 K calculated with the three functionals and compare them with the PBE results of Koči et al.²¹ There is a reasonable agreement between the two calculations especially at low pressure. At 3000 kbar our ECs are smaller than those of Koči et al. but quite close to them. At zero pressure, the pressure derivatives of the ECs are: $\frac{dC_{11}}{dp} = 5.8$, $\frac{dC_{12}}{dp} = 3.3$, $\frac{dC_{44}}{dp} = 1.3$, for all

FIG. 4. Adiabatic bulk and shear modulus of polycrystalline molybdenum against pressure computed at 5 K (red line), 300 K (green line), 1000 K (blue line), 1500 K (yellow line), and 2000 K (pink line), compared with room temperature experimental values of Ref.¹⁹ (red circles).

three functionals to be compared to the experimental values:¹⁸ $\frac{dC_{11}}{dp} = 6.41$, $\frac{dC_{12}}{dp} = 3.45$, and $\frac{dC_{44}}{dp} = 1.396$.

We show in Fig. 2 the QHA isothermal and adiabatic ECs compared with the adiabatic experimental values. Keeping into account the zero point motion on both the lattice constant and on the ECs themselves, we find $C_{11} = 4564$ kbar, $C_{12} = 1589$ kbar, and $C_{44} = 996$ kbar at 4 K, while computing the ECs from the strain derivatives of the energies at the lattice constant expanded by zero point motion effects within the QSA we get $C_{11} = 4593$ kbar, $C_{12} = 1565$ kbar, and $C_{44} = 996$ kbar.

As can be seen from Fig. 2, there is a good agreement between our calculated temperature dependence and the experimental data. From 24 K and 2022 K, the experimental values¹⁷ decrease of 1264 kbar (27 %), -63 kbar (-4 %), and 231 kbar (21 %) for C_{11} , C_{12} , and C_{44} respectively, while our

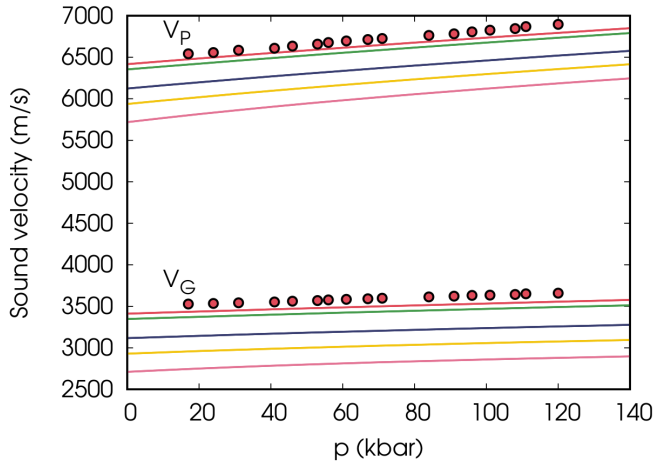


FIG. 5. Compressional and shear sound velocities of polycrystalline molybdenum against pressure at 5 K (red line), 300 K (green line), 1000 K (blue line), 1500 K (yellow line), and 2000 K (pink line), compared with room temperature experimental values of Ref.¹⁹ (red circles).

values decrease by 1400 kbar (31 %), -141 kbar (-9 %), and 287 kbar (29 %). In particular the increase of C_{12} with temperature is found also in our QHA calculation, slightly overestimated with respect to experiment.

For comparison we show in Fig. 3 the ECs calculated with the PBE functional within the QSA which are in good agreement with those calculated in Ref.²⁰. In this case, from 4 K to 2000 K, the decreases of C_{11} , C_{12} , and C_{44} are 380 kbar (8 %), 127 kbar (8 %), and 132 kbar (13 %). The decrease of C_{11} , and C_{44} is much smaller than in experiments (and within QHA) while C_{12} decreases with temperature instead of increasing as in experiment. We can understand this behaviour using the QHA ECs calculated at fixed volume that do not contain any thermal expansion effect. For these ECs C_{11} and C_{44} decrease with temperature, while C_{12} increases. Since QSA has only the effect of thermal expansion for C_{11} and C_{44} it misses the QHA contribution that give a larger decrease, while for C_{12} it has no increasing QHA term. The QHA predicts an almost constant C_{12} that is the results of the cancellation between the decrease due to thermal expansion and the increase due to the use of the free energy derivatives instead of the energy derivatives.

Using the QHA ECs we have calculated the properties of polycrystalline molybdenum. In Fig.3 we show the pressure dependence of the bulk modulus and of the shear modulus in the range of pressures (up to 140 kbar) measured in Ref.¹⁹. In addition to the 300 K calculation (green line), which can be compared with experiment, we show our predictions for 4 K, 1000 K, 1500 K and 2000 K. We can see that the derivatives of the bulk and shear modulus with respect to pressure are well followed by our curves. Our values at 300 K are $\frac{dB_S}{dp} = 4.24$ and $\frac{dG_S}{dp} = 1.33$ against experimental values (obtained by a linear fit) $\frac{dB_S}{dp} = 4.54$ and $\frac{dG_S}{dp} = 1.5$, respectively. These data are in agreement with the experimental values reported

in Ref.¹⁸: $\frac{dB_S}{dp} = 4.44$ and $\frac{dG_S}{dp} = 1.43$ and with the 0 K PBE theoretical results of Ref.¹⁹ $\frac{dB_S}{dp} = 4.4$ and $\frac{dG_S}{dp} = 1.7$. Regarding the temperature dependence of the adiabatic bulk and shear modulus we find the following derivatives at 298 K: $\frac{dB_S}{dT} = -0.15$ kbar/K and $\frac{dG_S}{dT} = -0.22$ kbar/K.

Finally using Eq. 9 and Eq. 10, we computed the compressional and shear sound velocities as a function of pressure for the same set of temperatures used in the previous picture. They are presented in Fig. 5. Even in this case the pressure dependence of the sound velocity at 300 K is well reproduced by the calculation and the other curves are our prediction.

IV. CONCLUSIONS

We presented the temperature and pressure dependent thermoelastic properties of molybdenum calculated by the `thermo_pw` software and PAW pseudopotentials. We find that the QHA predicts the temperature dependence of the ECs in much better agreement with experiments than the QSA. Furthermore we have used the QHA ECs to compute the pressure dependent compressional and shear sound velocities in polycrystalline molybdenum (and the corresponding bulk and shear moduli). In addition to the calculation at 300 K that is in good agreement with the experimental results of Liu et al.,¹⁹ we have calculated the low temperature (4 K) and the high temperature (1000 K, 1500 K, and 2000 K) pressure dependent curves, hoping that these calculations will stimulate an experimental investigation of these quantities.

For the sake of completeness, the phonon dispersions, the p-V equation of state at 300 K and 2000 K, the temperature dependent volume thermal expansion, the isobaric heat capacity, the adiabatic bulk modulus, and the average Grüneisen parameter for 0 kbar, 1000 kbar, 2000 kbar, and 3000 kbar have been calculated by the LDA, PBEsol, and PBE functionals, but since they are already available in the literature, we have moved them to the supplementary material.

V. SUPPLEMENTARY MATERIAL

Supplementary material that presents the calculated thermodynamic properties and a few tests on some numerical parameters are available at the following link:

ACKNOWLEDGMENTS

This work has been supported by the Italian MUR (Ministry of University and Research) through the National Centre for HPC, Big Data, and Quantum Computing (grant No. CN00000013). Computational facilities have been provided by SISSA through its Linux Cluster, ITCS, and the SISSA-CINECA 2021-2024 Agreement. Partial support has been received from the European Union through the MAX “MATERIALS design at the eXascale” Centre of Excellence for Supercomputing applications (Grant agreement No. 101093374,

co-funded by the European High Performance Computing joint Undertaking (JU) and participating countries 824143). X. Gong acknowledges the support received in the framework of the Joint Research Agreement for Magnetic Confinement Fusion between Eni and CNR.

- ¹L. Ming and M. H. Manghnani, *Journal of Applied Physics* **49**, 208 (1978).
- ²A. Dewaele, M. Torrent, P. Loubeyre, and M. Mezouar, *Physical Review B* **78**, 104102 (2008).
- ³Y. Zhao, A. C. Lawson, J. Zhang, B. I. Bennett, and R. B. Von Dreele, *Physical Review B* **62**, 8766 (2000).
- ⁴K. D. Litasov, P. I. Dorogokupets, E. Ohtani, Y. Fei, A. Shatskiy, I. S. Sharygin, P. N. Gavryushkin, S. V. Rashchenko, Y. V. Seryotkin, Y. Higo, K. Funakoshi, A. D. Chanyshv, and S. S. Lobanov, *Journal of Applied Physics* **113**, 093507 (2013).
- ⁵X. Huang, F. Li, Q. Zhou, Y. Meng, K. D. Litasov, X. Wang, B. Liu, and T. Cui, *Scientific Reports* **6**, 19923 (2016).
- ⁶R. S. Hixson and J. N. Fritz, *Journal of Applied Physics* **71**, 1721 (1992).
- ⁷F. C. Nix and D. MacNair, *Phys. Rev.* **61**, 74 (1942).
- ⁸V. Y. Bodryakov, *High Temperature* **52**, 840 (2014).
- ⁹Z.-Y. Zeng, C.-E. Hu, L.-C. Cai, X.-R. Chen, and F.-Q. Jing, *The Journal of Physical Chemistry B* **114**, 298 (2010).
- ¹⁰Z.-Y. Zeng, C.-E. Hu, X.-R. Chen, X.-L. Zhang, L.-C. Cai, and F.-Q. Jing, *Phys. Chem. Chem. Phys.* **13**, 1669 (2011).
- ¹¹Z.-Y. Zeng, C.-E. Hu, W. Zhang, Z.-W. Niu, and L.-C. Cai, *Journal of Applied Physics* **116**, 133518 (2014).
- ¹²Y. Wang, D. Chen, and X. Zhang, *Physical Review Letters* **84**, 3220 (2000).
- ¹³C. Cazorla, M. J. Gillan, S. Taioli, and D. Alfè, *The Journal of Chemical Physics* **126**, 194502 (2007).
- ¹⁴F. H. Featherston and J. R. Neighbours, *Physical Review* **130**, 1324 (1963).
- ¹⁵D. I. Bolef and J. de Klerk, *Journal of Applied Physics* **33**, 2311 (1962).
- ¹⁶J. M. Dickinson and P. E. Armstrong, *Journal of Applied Physics* **38**, 602 (1967).
- ¹⁷P. Bujard, R. Sanjines, E. Walker, J. Ashkenazi, and M. Peter, *Journal of Physics F: Metal Physics* **11**, 775 (1981).
- ¹⁸K. W. Katahara, M. H. Manghnani, and E. S. Fisher, *Journal of Physics F: Metal Physics* **9**, 773 (1979).
- ¹⁹W. Liu, Q. Liu, M. L. Whitaker, Y. Zhao, and B. Li, *Journal of Applied Physics* **106**, 043506 (2009).
- ²⁰Y. Wang, J. J. Wang, H. Zhang, V. R. Manga, S. L. Shang, L.-Q. Chen, and Z.-K. Liu, *J. Phys.: Condens. Matter* **22**, 225404 (2010).
- ²¹L. Koči, Y. Ma, A. R. Oganov, P. Souvatzis, and R. Ahuja, *Physical Review B* **77**, 214101 (2008).
- ²²A. Dal Corso, “thermo_pw,” can be found at the webpage https://github.com/dalcorso/thermo_pw (2014).
- ²³C. Malica and A. Dal Corso, *Journal of Physics: Condensed Matter* **32**, 315902 (2020).
- ²⁴C. Malica and A. Dal Corso, *Acta Crystallographica Section A* **75**, 624 (2019).
- ²⁵C. Malica and A. Dal Corso, *Journal of Applied Physics* **127**, 245103 (2020).
- ²⁶C. Malica and A. Dal Corso, *Journal of Physics: Condensed Matter* **33**, 475901 (2021).
- ²⁷X. Gong and A. Dal Corso, *Journal of Physics: Condensed Matter* **36**, 285702 (2024).
- ²⁸H. H. Pham, M. E. Williams, P. Mahaffey, M. Radovic, R. Arroyave, and T. Cagin, *Physical Review B* **84**, 064101 (2011), publisher: American Physical Society.
- ²⁹P. Haas, F. Tran, and P. Blaha, *Physical Review B* **79**, 085104 (2009).
- ³⁰T. S. Sokolova, P. I. Dorogokupets, and K. D. Litasov, *Russian Geology and Geophysics* **54**, 181 (2013).
- ³¹K. W. Katahara, M. H. Manghnani, L. C. Ming, and E. S. Fisher, *bcc transition metals under pressure: results from ultrasonic interferometry and diamond-cell experiments. [Nb–Mo, Ta–W]*, Tech. Rep. CONF-760716-4 (Argonne National Lab., IL (USA), 1976).
- ³²T. H. K. Barron and M. L. Klein, *Proceedings of the Physical Society* **85**, 523 (1965).
- ³³D. C. Wallace, *Thermodynamics of Crystals* (John Wiley and Sons, 1972).
- ³⁴A. Dal Corso, *Journal of Physics: Condensed Matter* **28**, 075401 (2016).
- ³⁵M. Palumbo and A. Dal Corso, *Physica Status Solidi (B)* **254**, 1700101 (2017).
- ³⁶P. Giannozzi, S. Baroni, N. Bonini, M. Calandra, R. Car, C. Cavazzoni, D. Ceresoli, G. L. Chiarotti, M. Cococcioni, I. Dabo, A. D. Corso, S. d. Gironcoli, S. Fabris, G. Fratesi, R. Gebauer, U. Gerstmann, C. Gougoussis, A. Kokalj, M. Lazzeri, L. Martin-Samos, N. Marzari, F. Mauri, R. Mazzarello, S. Paolini, A. Pasquarello, L. Paulatto, C. Sbraccia, S. Scandolo, G. Sclauzero, A. P. Seitsonen, A. Smogunov, P. Umari, and R. M. Wentzcovitch, *Journal of Physics: Condensed Matter* **21**, 395502 (2009).
- ³⁷P. Giannozzi, O. Andreussi, T. Brumme, O. Bunau, M. Buongiorno Nardelli, M. Calandra, R. Car, C. Cavazzoni, D. Ceresoli, M. Cococcioni, N. Colonna, I. Carnimeo, A. Dal Corso, S. de Gironcoli, P. Delugas, R. A. DiStasio, A. Ferretti, A. Floris, G. Fratesi, G. Fugallo, R. Gebauer, U. Gerstmann, F. Giustino, T. Gorni, J. Jia, M. Kawamura, H.-Y. Ko, A. Kokalj, E. Küçükbenli, M. Lazzeri, M. Marsili, N. Marzari, F. Mauri, N. L. Nguyen, H.-V. Nguyen, A. Otero-de-la Roza, L. Paulatto, S. Poncé, D. Rocca, R. Sabatini, B. Santra, M. Schlipf, A. P. Seitsonen, A. Smogunov, I. Timrov, T. Thonhauser, P. Umari, N. Vast, X. Wu, and S. Baroni, *Journal of Physics: Condensed Matter* **29**, 465901 (2017).
- ³⁸J. P. Perdew and A. Zunger, *Physical Review B* **23**, 5048 (1981).
- ³⁹J. P. Perdew, A. Ruzsinszky, G. I. Csonka, O. A. Vydrov, G. E. Scuseria, L. A. Constantin, X. Zhou, and K. Burke, *Physical Review Letters* **100**, 136406 (2008).
- ⁴⁰J. P. Perdew, K. Burke, and M. Ernzerhof, *Physical Review Letters* **77**, 3865 (1996).
- ⁴¹P. E. Blöchl, *Physical Review B* **50**, 17953 (1994).
- ⁴²A. Dal Corso, “pslibrary,” can be found at the webpage <https://github.com/dalcorso/pslibrary> (2010).
- ⁴³S. G. Louie, S. Froyen, and M. L. Cohen, *Phys. Rev. B* **26**, 1738 (1982).
- ⁴⁴M. Methfessel and A. T. Paxton, *Physical Review B* **40**, 3616 (1989).
- ⁴⁵S. Baroni, S. de Gironcoli, A. Dal Corso, and P. Giannozzi, *Review of Modern Physics* **73**, 515 (2001).
- ⁴⁶A. Dal Corso, *Physical Review B* **81**, 075123 (2010).
- ⁴⁷X. Gong and A. Dal Corso, “unpublished,” (2023).

Supplementary material for: **Ab initio quasi-harmonic thermoelasticity of molybdenum under high temperature and pressure**

Xuejun Gong^{1,2, a)} and Andrea Dal Corso^{1,2, b)}

¹⁾*International School for Advanced Studies (SISSA), Via Bonomea 265, 34136, Trieste, Italy*

²⁾*IOM - CNR, Via Bonomea 265, 34136, Trieste, Italy*

(Dated: 25 June 2024)

This supplementary material documents the phonon dispersions, thermal expansion, isobaric heat capacity, adiabatic bulk modulus, and average Grüneisen parameter of molybdenum under high temperature and pressure, calculated by `thermo_pw` with three exchange and correlation functionals (LDA¹, PBEsol², and PBE³). Available results from experiments and previous calculations are also marked on the figures for reference.

^{a)}xgong@sissa.it

^{b)}dalcorso@sissa.it

I. THEORY

We start by summarizing the thermodynamic relationships used in this supplementary material.

Considering p as a fixed parameter, the minimization of the functional $G_p(V, T) = F(V, T) + pV$ with respect to the volume gives the equation of state (EOS):

$$p = -\frac{\partial F(V, T)}{\partial V}. \quad (1)$$

Hence the volume that minimizes $G_p(V, T)$ is the volume at pressure p and temperature T : $V(p, T)$. Using $V(p, T)$ we obtain the volume thermal expansion $\beta_V(p, T)$ at pressure p as:

$$\beta_V(p, T) = \frac{1}{V(p, T)} \left. \frac{\partial V(p, T)}{\partial T} \right|_p. \quad (2)$$

Using $p(V, T)$ (Eq. 1), we compute the isothermal bulk modulus as:

$$B_T(V, T) = -V \left. \frac{\partial p(V, T)}{\partial V} \right|_T = V \left. \frac{\partial^2 F(V, T)}{\partial V^2} \right|_T. \quad (3)$$

The part of the bulk modulus B_T that derives from $U(V)$ is a parameter of the Birch-Murnaghan equation, while the thermal part which derives from $F_{ph} + F_{el}$ is calculated by a second volume derivative of the polynomial interpolation.

The vibrational contribution to the isochoric heat capacity $C_{V,ph}(V, T)$ is calculated for the N_V geometries by:

$$C_{V,ph}(V, T) = \frac{1}{N} \sum_{\mathbf{q}, \eta} \hbar \omega_{\eta}(\mathbf{q}, V) \frac{\partial}{\partial T} \left[\frac{1}{e^{\beta \hbar \omega_{\eta}(\mathbf{q}, V)} - 1} \right]. \quad (4)$$

The electronic contribution $C_{V,el}(V_i, T)$ is computed from the electronic density of states and is added to $C_{V,ph}(V_i, T)$ to obtain $C_V(V_i, T) = C_{V,ph}(V_i, T) + C_{V,el}(V_i, T)$. At each temperature, these quantities are fitted by a fourth-degree polynomial in V . The isobaric heat capacity is given by:

$$C_p(p, T) = C_V(V, T) + \beta_V^2(p, T) B_T(V, T) V T, \quad (5)$$

the adiabatic bulk modulus is:

$$B_S(p, T) = B_T(V, T) + \frac{\beta_V^2(p, T) B_T^2(V, T) V T}{C_V(V, T)}, \quad (6)$$

and the thermodynamic average Grüneisen parameter is defined as:

$$\gamma(p, T) = \frac{\beta_V(p, T) B_T(V, T) V}{C_V(V, T)}. \quad (7)$$

In the present supplementary material, in addition to $\beta_V(p, T)$, we show $C_p(p, T)$, $B_S(p, T)$, and $\gamma(p, T)$ for several pressures p , so when V appears in Eqs. 5-7 we use $V(p, T)$.

II. RESULTS

A. Phonon dispersion

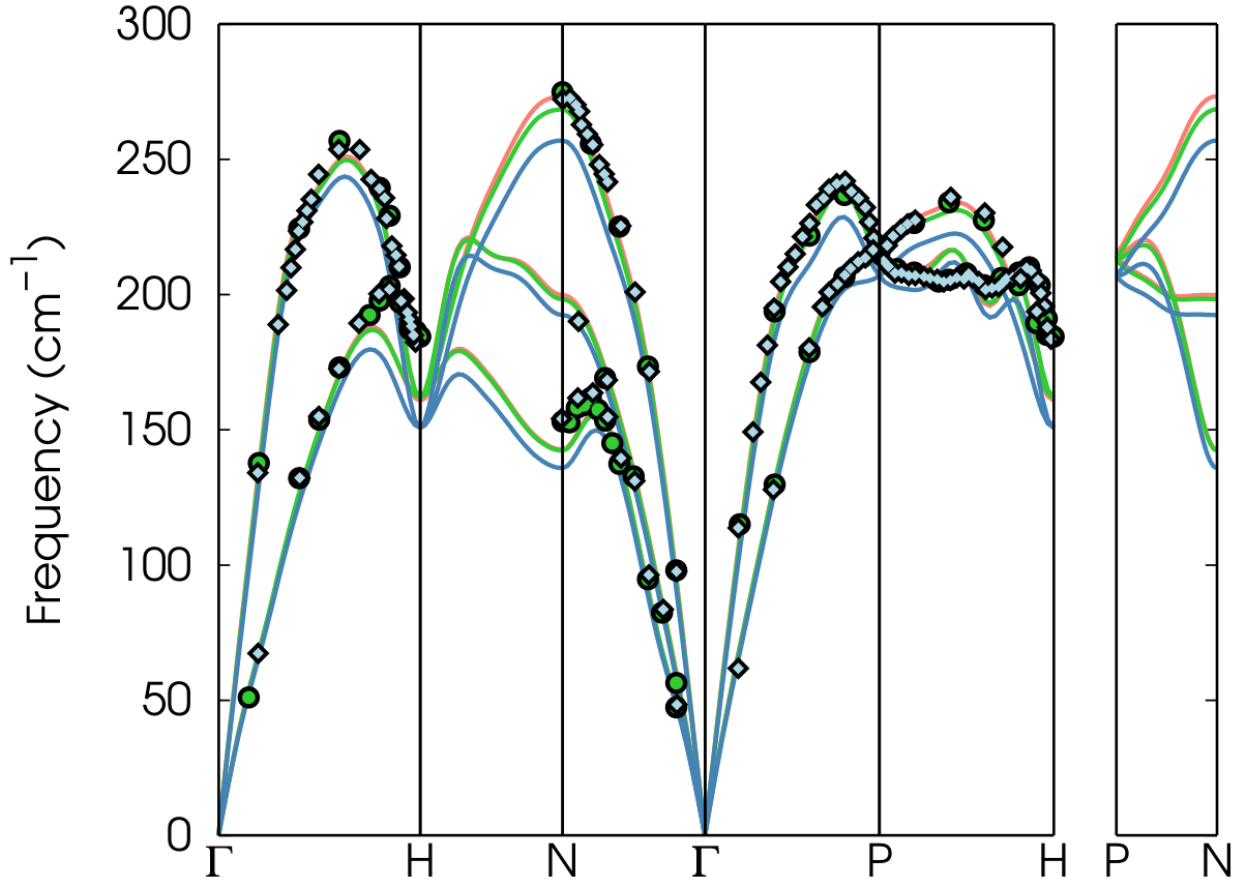


FIG. 1. Phonon dispersions interpolated at the 295 K lattice constant. The LDA (red curves), PBEsol (green curve), and PBE (blue curve) results are compared with the experimental inelastic neutron scattering data measured at 295 K (Ref.⁴ blue diamonds and Ref.⁵ green circles).

In Fig. 1, we compare the theoretical phonon dispersions, interpolated at the 295 K lattice constant obtained accounting for zero point and thermal expansion effects (see the

values in Table 1 of the paper), with inelastic neutron scattering data.^{4,5} LDA and PBEsol give similar frequencies in good agreement with experiment except at the H point where we find a relatively large error. PBE gives frequencies lower than LDA (as found in other solids^{6,7}), and hence more distant from experiment. As for gold, platinum and tungsten, for molybdenum phonon dispersions, LDA or PBEsol are preferable to PBE. This conclusion is in agreement with Ref.^{7,8}. Instead, Ref.⁹ finds PBE phonon dispersions closer to experiment than ours.

B. Thermal equation of state

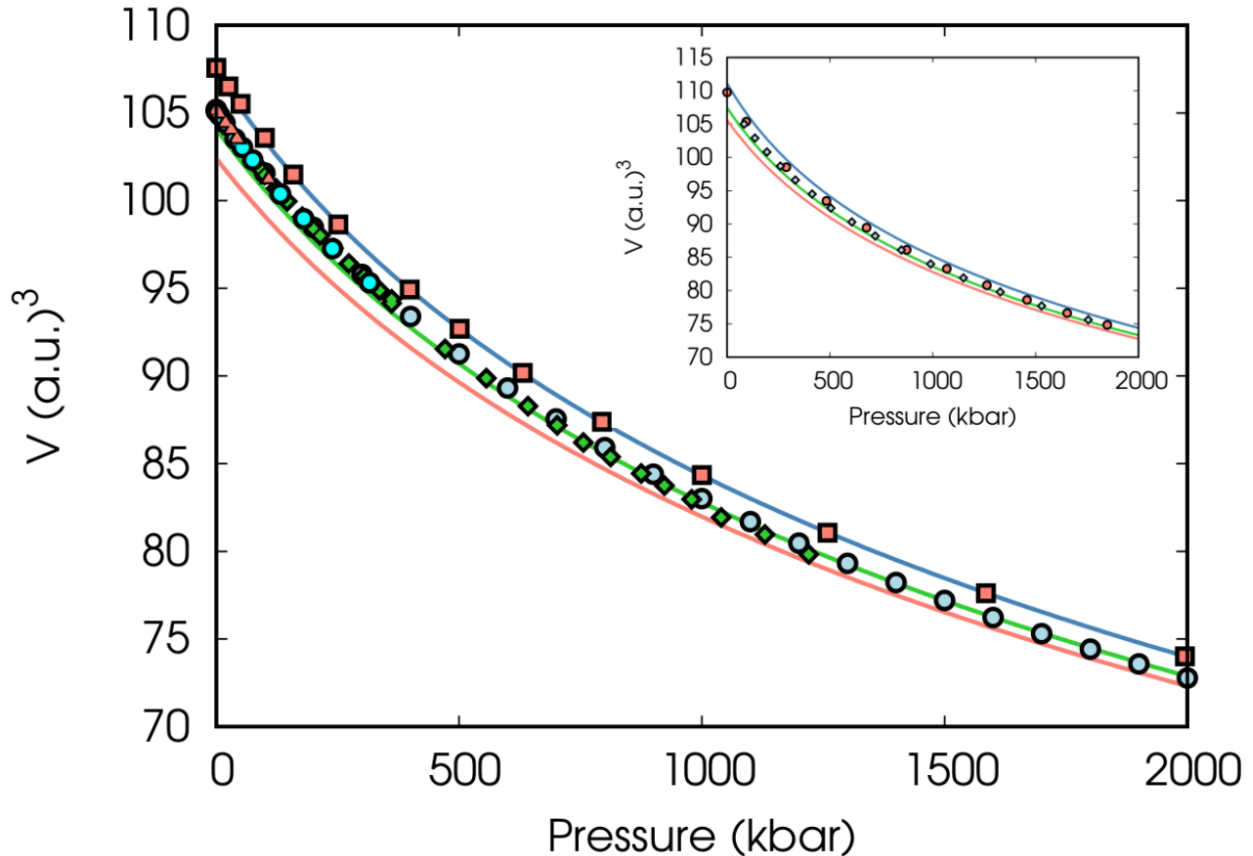


FIG. 2. V as a function of p at 300 K obtained by LDA (red), PBEsol (green), and PBE (blue) compared with experiment (blue circles¹⁰, cyan circles,¹¹ red triangles,¹² and green diamonds¹³) and previous calculations (red squares (PBE) from Ref.¹⁴). In the inset the same curves at 2000 K compared with the predictions of Ref.¹¹ (red circles) and of Ref.¹⁵ (blue diamonds).

In Fig. 2, we show the 300 K equation of state. Our PBE curve agrees with the linearized augmented plane wave (LAPW) all-electrons PBE calculation of Ref.¹⁴ and with the PW91¹⁶ results of Ref.⁹. The experimental results are all in good agreement among themselves with the shock wave data arriving beyond 2000 kbar. At each pressure, the PBE curve overestimates the volume, while LDA underestimate it as we have discussed for zero pressure. The PBEsol volume is still slightly underestimated at zero pressure, but the agreement with experiment increases with pressure. The same behaviour is found at 2000 K as we show in the inset. Here we compare our equation of state with the models of Ref.^{15,17} and¹¹. The two models agree with each other and with the ab-initio results especially using PBE and PBEsol.

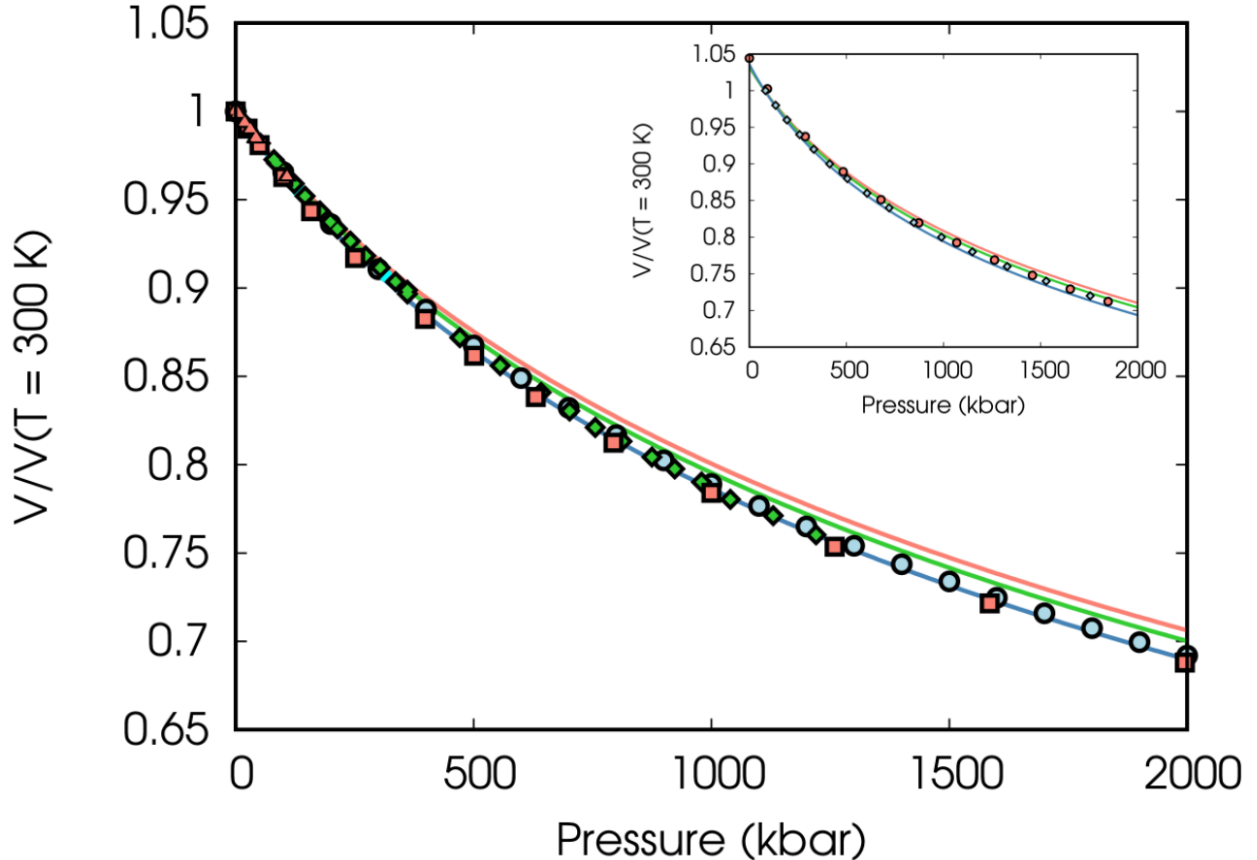


FIG. 3. V/V_0 as a function of p at 300 K obtained by LDA (red), PBEsol (green), and PBE (blue) compared with experiment (blue circles¹⁰, cyan circles,¹¹ red triangles,¹² and green diamonds¹³) and previous PBE calculations (red¹⁴ squares). In the inset the same curves at 2000 K compared with the predictions of Ref.¹¹ (red circles) and of Ref.¹⁵ (blue diamonds).

In Fig. 3 we present the equation of state removing the error due to the equilibrium volume by plotting V/V_0 as a function of pressure (here V_0 is the equilibrium volume at 300 K, close to that reported in Table 1 of the paper). As in the case of tungsten, here the picture changes, with PBE that follows the experimental data in all the pressure range. Both LDA and PBEsol are in this case slightly above the experiment. In the inset we show the equation of state at 2000 K and compare with the model data presented in the inset of Fig. 2. At this temperature the model points are equally close to PBE and PBEsol. At zero pressure the theoretical data are slightly below the model point of Ref.¹¹ reflecting the underestimation of the thermal expansion with respect to experiment (see below).

C. Thermal expansion

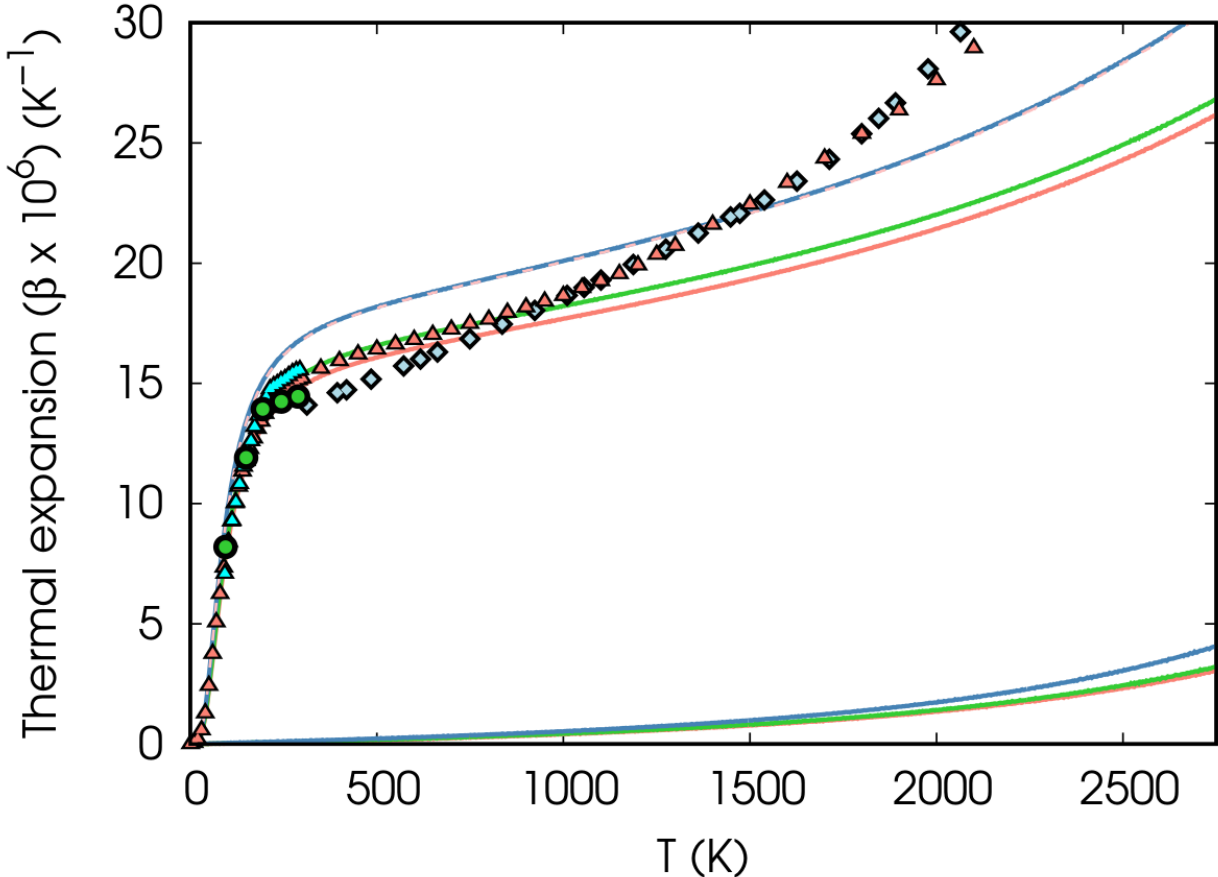


FIG. 4. Temperature dependent thermal expansion calculated by LDA (red curve), PBEsol (green curve), and PBE (blue curve) compared with the experimental data reported in Ref.¹⁸ (cyan triangles) Ref.¹⁹ (green circles), Ref.²⁰ (blue diamonds), Ref.²¹ (red triangles). The thinner lines at the bottom indicate the differences between the thermal expansion calculated including or neglecting the electronic excitations term in the free energy. Pink dashed line on the PBE curve shows the result obtained with 8 geometries and $\Delta a = 0.02$ a.u.

In Fig. 4, we compare with experiment the thermal expansion at zero pressure. We have reported only the commonly accepted data, as those of Refs.¹⁸⁻²¹ and not the new measurements proposed by Ref.¹². Our LDA and PBEsol data match the accepted values up to 1000 K while PBE is slightly higher. The PW91 data of Ref.⁹ (not reported here) are more close to our LDA data, than to the PBE data and match the experimental thermal

expansion up to 1500 K. After these temperatures, anharmonic phonon-phonon interaction effects are expected to become important and therefore our ab-initio data cannot follow experiment. In the picture we show also the electronic excitation contribution to the thermal expansion, calculated adding or neglecting the electronic term in the free energy. As can be seen from the figure at 3000 K it is of the order of $5 \cdot 10^{-6}$ (1/K), but at 1500 K its contribution is negligible.

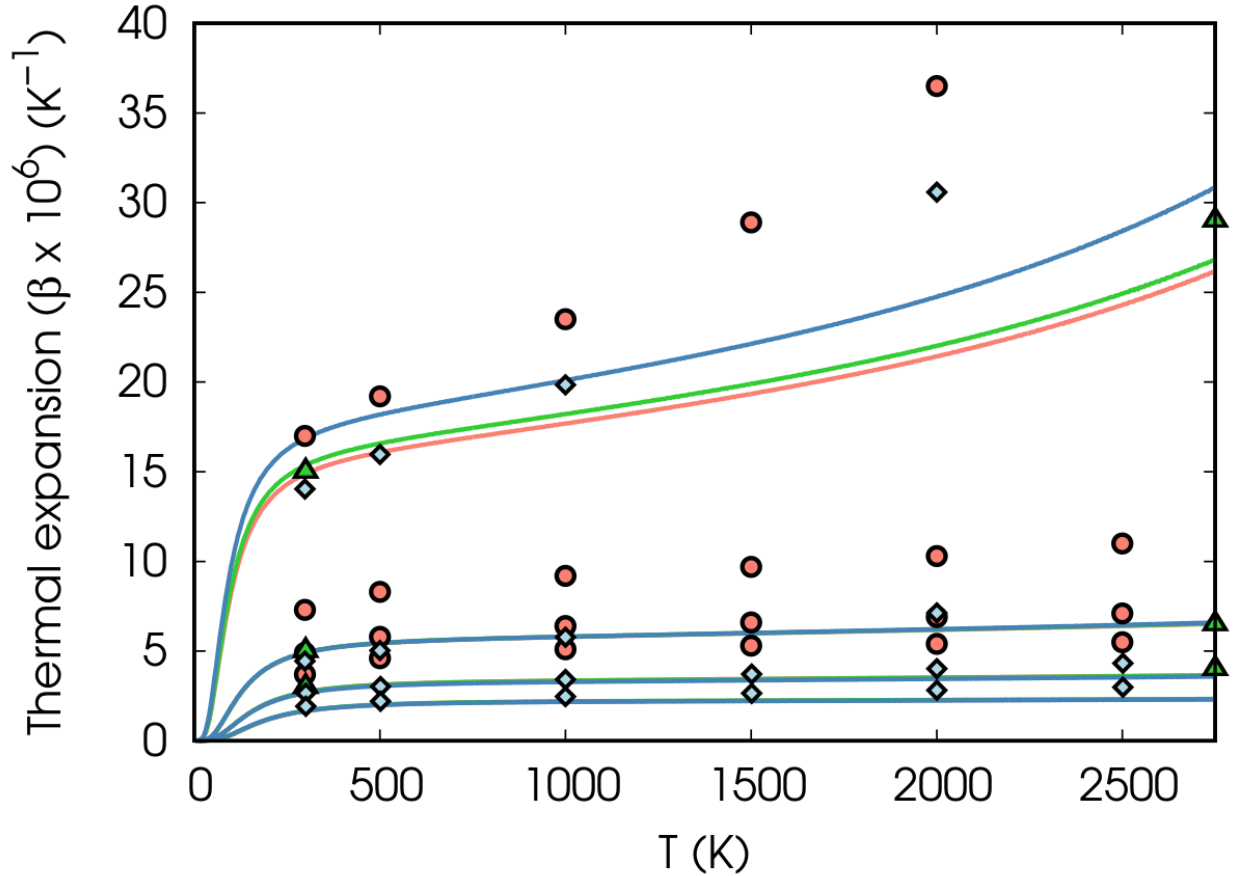


FIG. 5. Temperature dependent thermal expansion computed within the LDA (red line), PBEsol (green line), and PBE (blue line). The different curves (from top to bottom) correspond to pressures from 0 kbar to 3000 kbar in steps $\Delta p = 1000$ kbar. Theory is compared with the models of Ref.¹¹ (red circles) and of Ref.¹⁷ (blue diamonds) and with the ab-initio PBE calculations of Ref.⁹ (green triangles).

In Fig. 5, we show the thermal expansion at 0 kbar, 1000 kbar, 2000 kbar, and 3000 kbar and compare our data with the models of Ref.¹¹ and of Ref.¹⁷. For the first we use the data reported in their Tab. V, while for the latter we use the data reported in Tab. 7 for 0 kbar

and 1000 kbar and data calculated by us with the parameters reported at pag.193 at 2000 kbar and 3000 kbar. In the same figure we report also the PW91 values of Ref.⁹. We find that the three functionals differ appreciably at 0 kbar, but the differences are smaller at higher pressures. The pressure dependence of the thermal expansion agrees with the PW91 findings of Ref.⁹. The points of the two models differ at high pressure, with the model of Ref.¹¹ that decreases more slowly with pressure. Our data agree very well with the model of Ref.¹⁷ until about 1000 K, but our curves are below the model points at higher temperatures. This seems due to missing anharmonic phonon-phonon interaction terms in our calculation.

D. Heat capacity

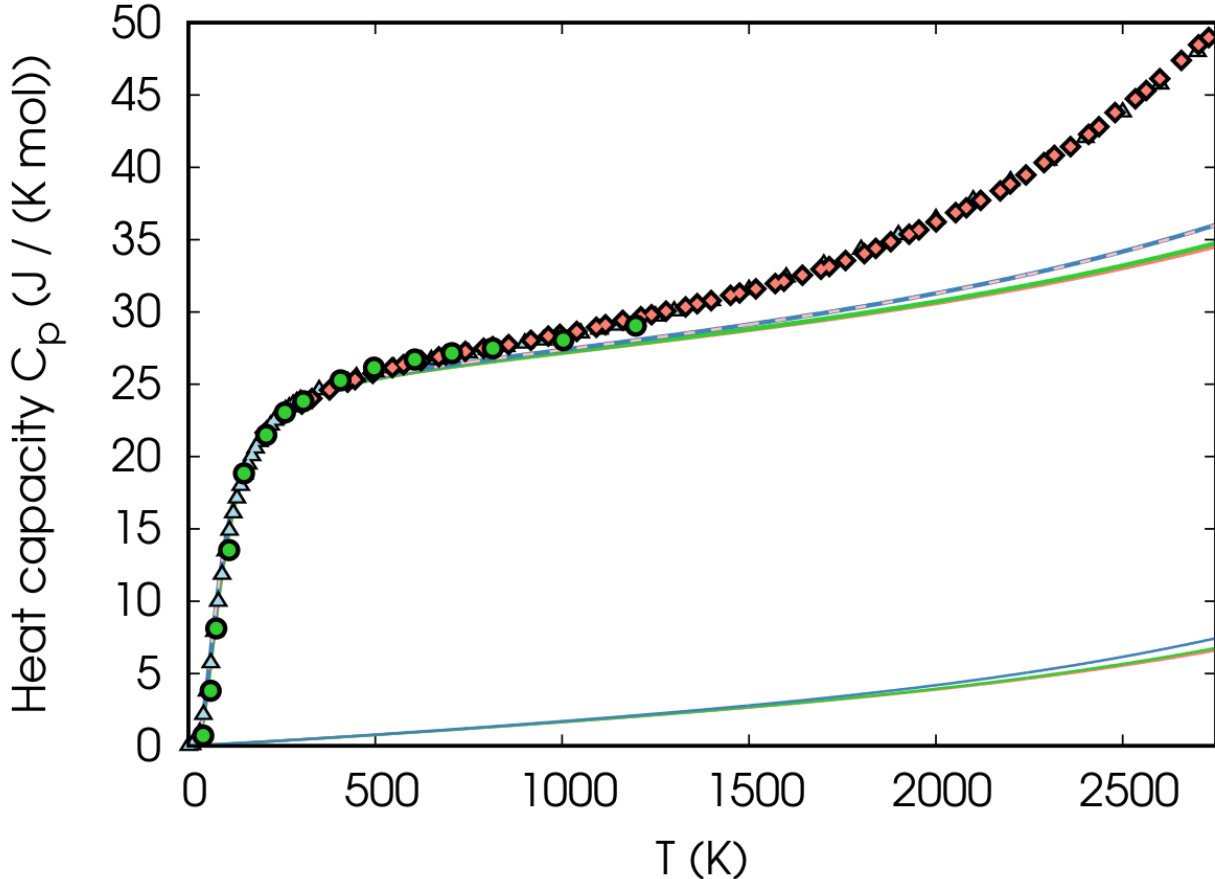


FIG. 6. LDA (red line), PBEsol (green line), and PBE (blue line) temperature dependent isobaric heat capacity compared with experiment from Ref.¹⁹ (green circles), Ref.²² (red diamonds) and Ref.²¹ (blue triangles). Thin lines at the bottom (with the same color conventions) indicate the contribution of electronic thermal excitations to the heat capacity. Pink dashed line on the PBE curve shows the result obtained with 8 geometries and $\Delta a = 0.02$ a.u.

In Fig. 6, we compare the isobaric heat capacity with experiment. The three functionals gives very similar values of this quantity and theory and experiment are in good agreement until about 1000 K. As can be seen from the figure at 2500 K our value of 33.2 J/(K· mol) has a contribution of electronic excitation of about 5.7 J/(K· mol), while the quasiharmonic term contributes for other 2.5 J/(K· mol), while the experimental value is 44.1 J/(K· mol) so that the anharmonic phonon-phonon interaction and possibly defects should give a contribution

of about $10.9 \text{ J}/(\text{K} \cdot \text{mol})$.

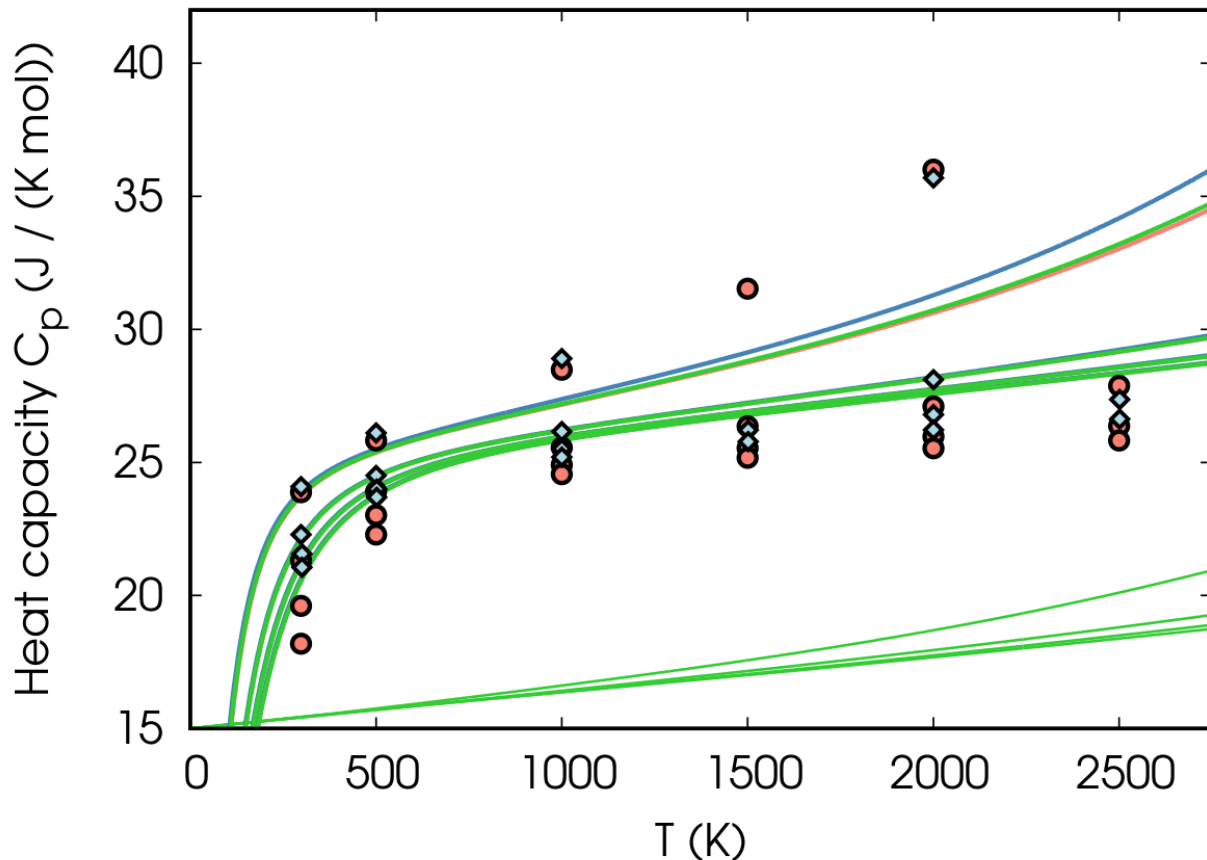


FIG. 7. LDA (red line), PBEsol (green line), and PBE (blue line) temperature dependent isobaric heat capacity. From top to bottom the curves correspond to pressures from 0 kbar to 3000 kbar in steps $\Delta p = 1000$ kbar. DFT calculations are compared with the model of Ref.¹¹ (red circles) and of Ref.¹⁵ (blue diamond). The green lines at the bottom are the PBEsol electronic contribution to C_V at the four pressures (from top to bottom) shifted by $15 \text{ J}/(\text{K} \cdot \text{mol})$.

In Fig. 7, we report the isobaric heat capacity at several pressures. In the same figure we show also the electronic contribution to which we added a fixed value of $15 \text{ J}/(\text{K} \cdot \text{mol})$ for picture clarity. At zero pressure both models gives very similar results which reproduce well experiment, but the behaviour with pressure is different, with the model of Ref.¹¹ which converges faster to the Dulong-Petit limit. We find that the electronic contribution decrease slowly with pressure and added to the Dulong-Petit value gives a C_p higher than the point of Ref.¹¹. It seems therefore that this model somewhat underestimates the electronic contribution to the specific heat at high pressures.

E. Bulk modulus

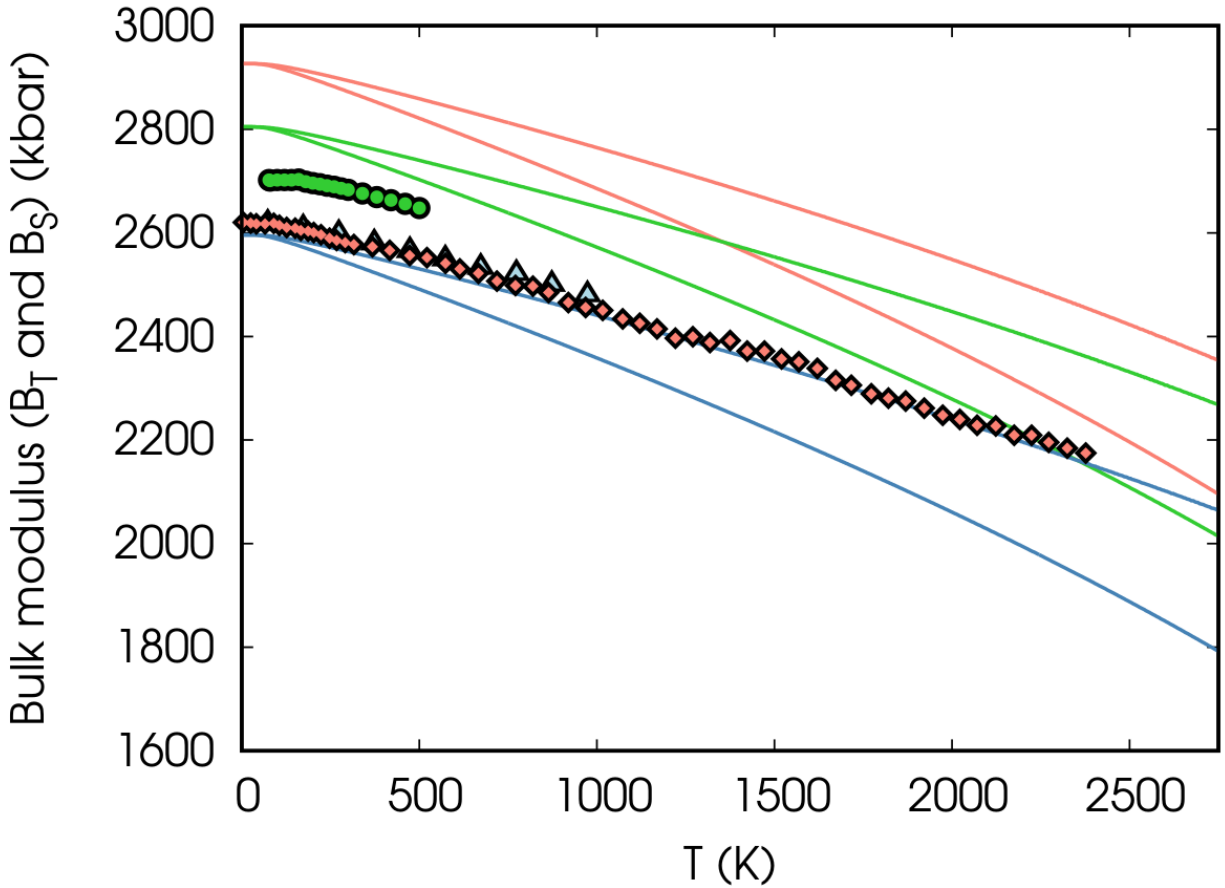


FIG. 8. Temperature dependent adiabatic and isothermal bulk moduli calculated within LDA (red line), PBEsol (green line), and PBE (blue line) compared with the experimental adiabatic data of Ref.²³ (blue triangles), Ref.²⁴ (green circles) and Ref.²⁵ (red diamonds). For each functional the higher curve is the adiabatic bulk modulus.

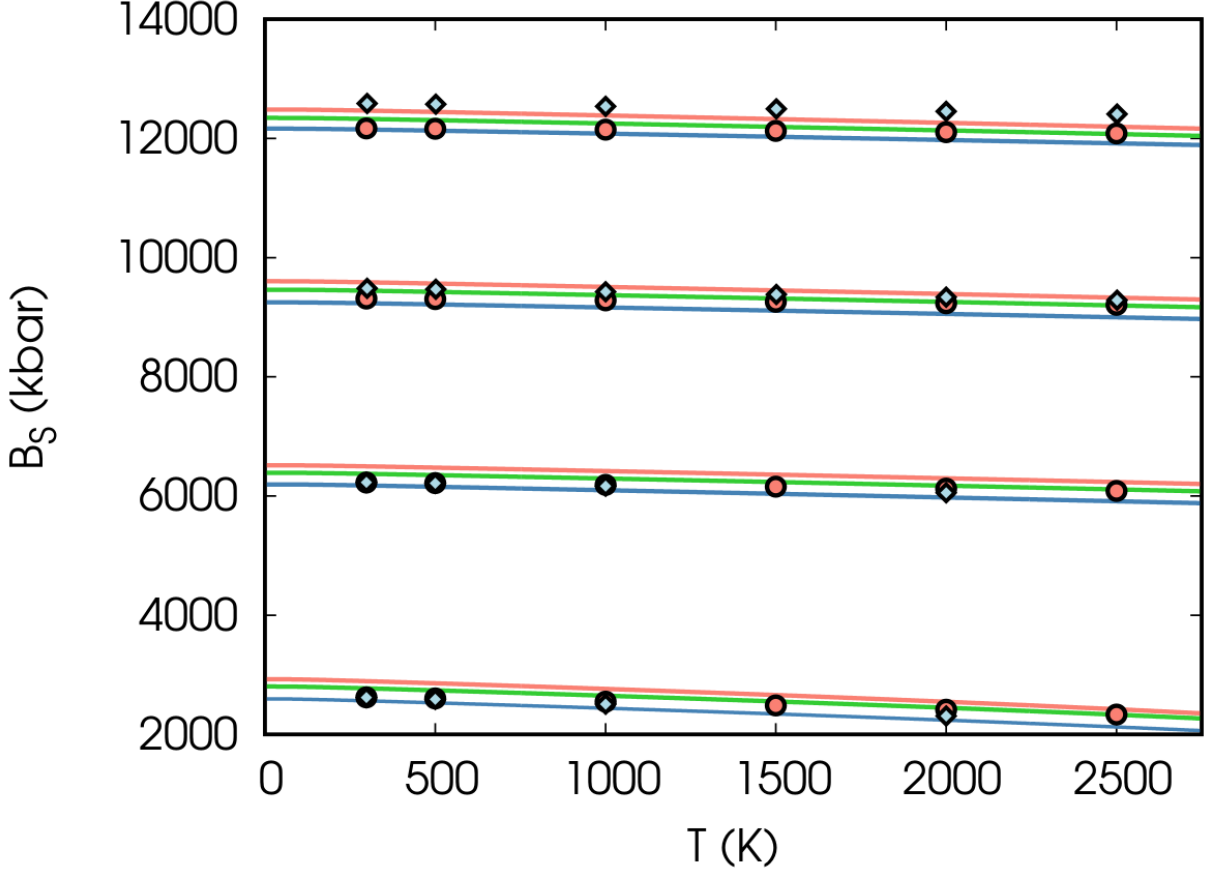


FIG. 9. Temperature dependent adiabatic bulk modulus calculated within the LDA (red lines), PBEsol (green lines), and PBE (blue lines). From bottom to top the curves correspond to pressures from 0 kbar to 3000 kbar in steps $\Delta p = 1000$ kbar. DFT calculations are compared with the model predictions of Ref.¹¹ (red circles) and of Ref.¹⁷ (blue diamond).

In Fig. 8, we compare the adiabatic bulk modulus with experiment. The isothermal bulk modulus is plotted for reference. The PBE bulk modulus is in very good agreement with experiment and also the temperature dependence seems to be well accounted for by theory. LDA and PBEsol instead overestimate the bulk modulus. The decrease of the experimental bulk modulus from 25 K to 2225 K is 410 kbar (16 %), while the LDA, PBEsol, and PBE values are 432 (15 %), 407 kbar (15 %), and 405 kbar (16 %), respectively. In Fig. 9, we report the adiabatic bulk modulus at several pressures. Our data are compared with the models of Ref.¹¹ and of Ref.¹⁵ (only at 0 kbar and 1000 kbar). In all the range of pressures the agreement between ab-initio values and model values is very good with PBE which remain always quite close to the model points and PBEsol and PBE slightly above. For this

quantity the differences between functionals do not decrease with pressure.

F. Grüneisen parameter

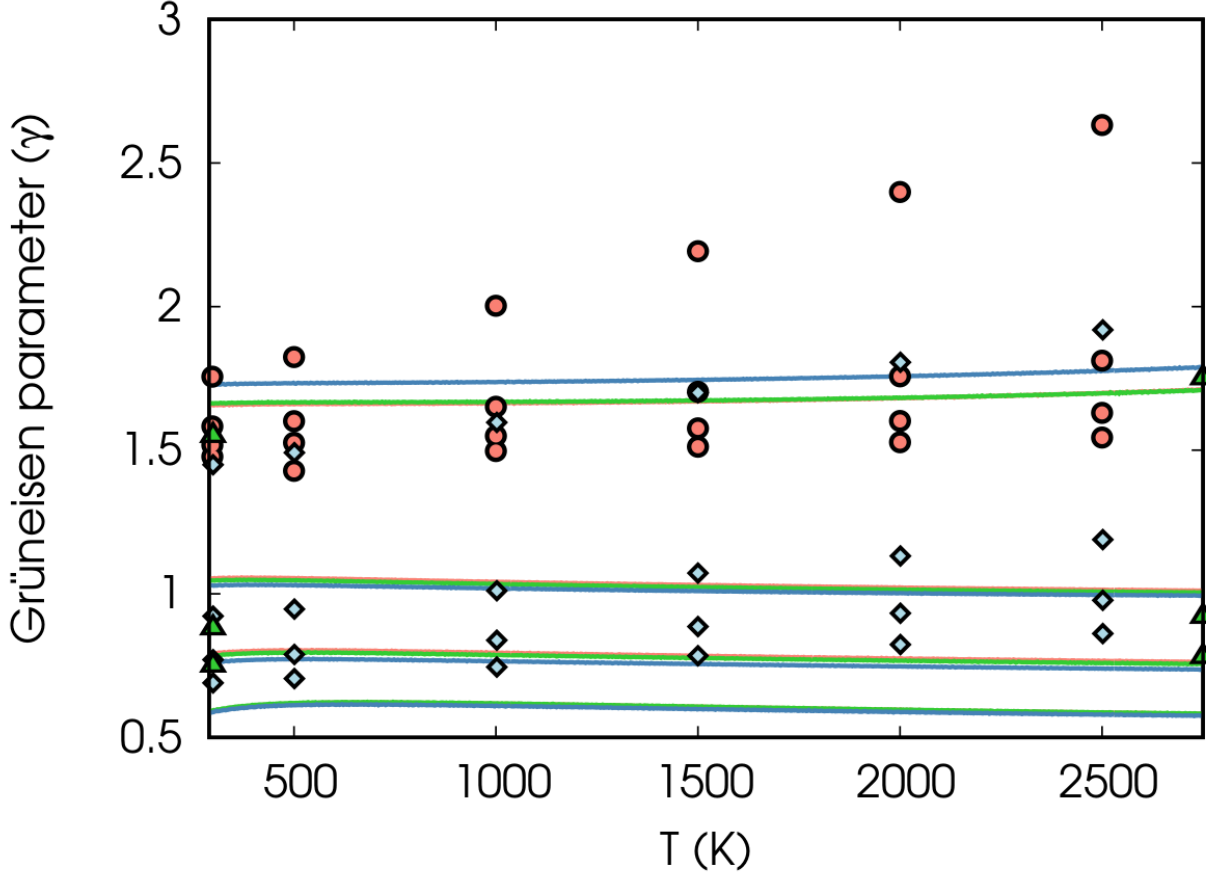


FIG. 10. Temperature dependent average Grüneisen parameter calculated within the LDA (red line below the green line), PBEsol (green line) and PBE (blue line). From top to bottom the curves correspond to pressures from 0 kbar to 3000 kbar in steps $\Delta p = 1000$ kbar. DFT calculations are compared with the model predictions of Ref.¹¹ (red circles) and of Ref.¹⁵ (blue diamond) and with the ab-initio PBE calculations of Ref.⁹ (green triangles).

In Fig. 10, we report the average Grüneisen parameter as a function of temperature and compare it with previous ab-initio calculation⁹ and with the model data of Ref.¹¹ and of Ref.¹⁵. The agreement with the PW91 calculation is quite good especially at high pressure. The major difference is at 0 kbar and 300 K where the value of Ref.⁹ is closer to the model of Ref.¹⁵ while our value is closer to the model Ref.¹¹. With temperature the model data and

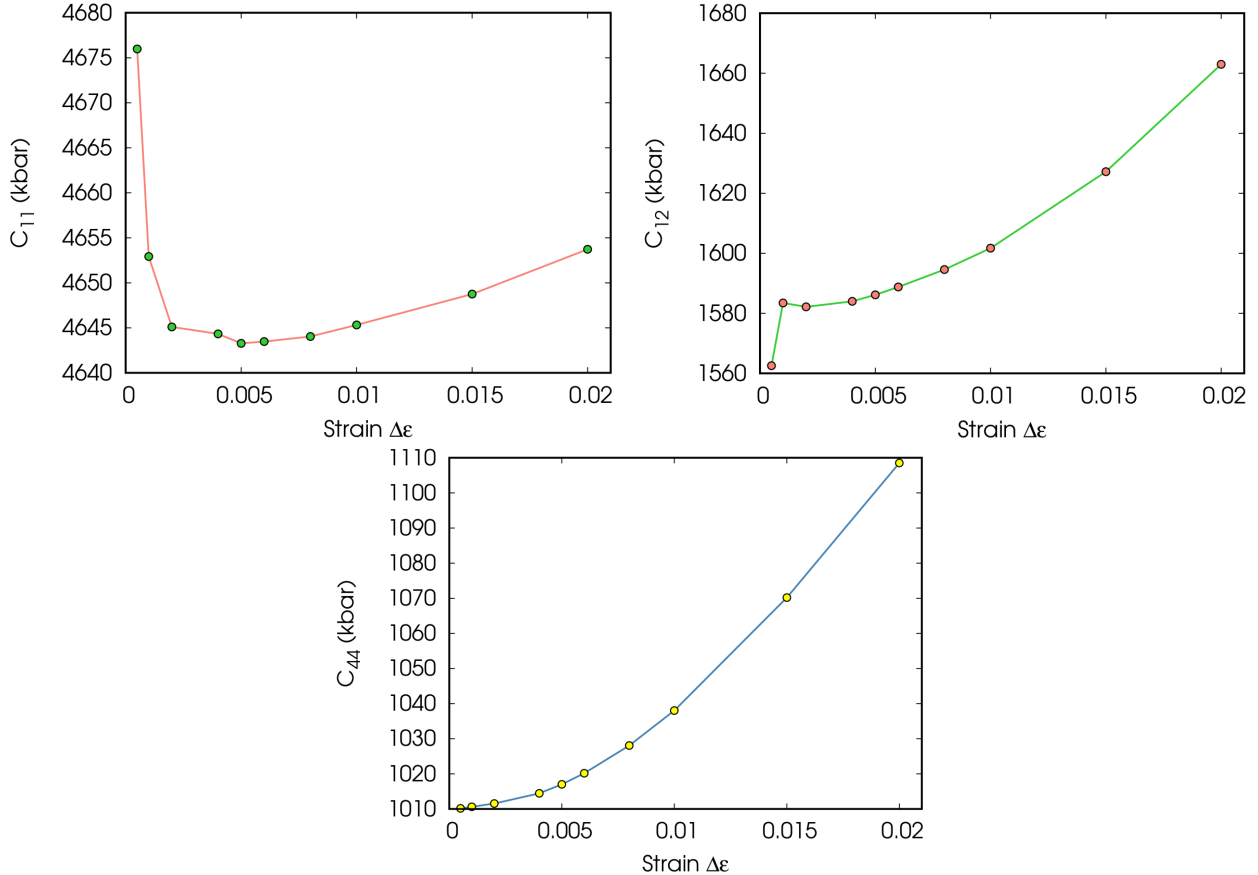


FIG. 11. Value of the $T = 0$ K elastic constants calculated with different values of the strain interval for each strain type.

the ab-initio calculation increase faster than our values and at 0 kbar and 2750 K our value coincide with previous ab-initio result, but remains lower than both models. The model of Ref.¹¹ has average Grüneisen parameters decreasing much slowly with pressure than both the ab-initio results and the model of Ref.¹⁵. The ab-initio results however seems to remain more constant with temperature than the results of Ref.¹⁵. This in part could be due to the missing anharmonic phonon-phonon terms in the ab-initio calculation.

III. NUMERICAL ISSUES

The choice of the interval between strains used to sample the energy might affect the final value of the elastic constants. We show in Fig. 11 the dependence of the three elastic constants on this parameter. As can be seen from the figure, when the strain interval is small enough to avoid the high order terms in the energy versus strain curves that appear

at large $\Delta\varepsilon$, the values of the elastic constants converge to a constant value. In principle, we should compute the limit for $\Delta\varepsilon \rightarrow 0$, but as can be seen in the curve for C_{11} , if the value of $\Delta\varepsilon$ is too small, the fit of the energy becomes also inaccurate. In the paper we used a value $\Delta\varepsilon = 0.005$, that gives values of elastic constants close to the limit of small $\Delta\varepsilon$ without introducing significant errors. We note that in these figures we are using an enlarged scale, but on the scale of elastic constants used in the paper, these curves appear almost flat.

We have also studied the dependence of our thermodynamic properties on the distance Δa among the geometries used to compute phonons. The Δa used in the paper is 0.1 a.u., but also a $\Delta a = 0.2$ a.u. gives very similar results as we show for PBE in Fig. 4 and in Fig. 6.

REFERENCES

- ¹J. P. Perdew and A. Zunger, “Self-interaction correction to density-functional approximations for many-electron systems,” *Physical Review B* **23**, 5048–5079 (1981).
- ²J. P. Perdew, A. Ruzsinszky, G. I. Csonka, O. A. Vydrov, G. E. Scuseria, L. A. Constantin, X. Zhou, and K. Burke, “Restoring the density-gradient expansion for exchange in solids and surfaces,” *Physical Review Letters* **100**, 136406 (2008).
- ³J. P. Perdew, K. Burke, and M. Ernzerhof, “Generalized gradient approximation made simple,” *Physical Review Letters* **77**, 3865–3868 (1996).
- ⁴B. M. Powell, P. Martel, and A. D. B. Woods, “Lattice dynamics of niobium-molybdenum alloys,” *Physical Review* **171**, 727–736 (1968).
- ⁵J. Zarestky, C. Stassis, B. N. Harmon, K. M. Ho, and C. L. Fu, “Temperature dependence of the vibrational modes of molybdenum,” *Physical Review B* **28**, 697–701 (1983).
- ⁶A. Dal Corso, “Ab initio phonon dispersions of transition and noble metals: effects of the exchange and correlation functional,” *Journal of Physics: Condensed Matter* **25**, 145401 (2013).
- ⁷S. Y. Savrasov and D. Y. Savrasov, “Electron-phonon interactions and related physical properties of metals from linear-response theory,” *Physical Review B* **54**, 16487–16501 (1996).
- ⁸C. Cazorla, M. J. Gillan, S. Taioli, and D. Alfè, “Melting curve and hugoniot of molybdenum up to 400 GPa by ab initio simulations,” *Journal of Physics: Conference Series* **121**,

- 012009 (2008).
- ⁹Z.-Y. Zeng, C.-E. Hu, L.-C. Cai, X.-R. Chen, and F.-Q. Jing, “Lattice dynamics and thermodynamics of molybdenum from first-principles calculations,” *The Journal of Physical Chemistry B* **114**, 298–310 (2010).
- ¹⁰R. S. Hixson and J. N. Fritz, “Shock compression of tungsten and molybdenum,” *Journal of Applied Physics* **71**, 1721–1728 (1992).
- ¹¹K. D. Litasov, P. I. Dorogokupets, E. Ohtani, Y. Fei, A. Shatskiy, I. S. Sharygin, P. N. Gavryushkin, S. V. Rashchenko, Y. V. Seryotkin, Y. Higo, K. Funakoshi, A. D. Chanyshhev, and S. S. Lobanov, “Thermal equation of state and thermodynamic properties of molybdenum at high pressures,” *Journal of Applied Physics* **113**, 093507 (2013).
- ¹²Y. Zhao, A. C. Lawson, J. Zhang, B. I. Bennett, and R. B. Von Dreele, “Thermoelastic equation of state of molybdenum,” *Physical Review B* **62**, 8766–8776 (2000).
- ¹³A. Dewaele, M. Torrent, P. Loubeyre, and M. Mezouar, “Compression curves of transition metals in the mbar range: Experiments and projector augmented-wave calculations,” *Physical Review B* **78**, 104102 (2008).
- ¹⁴Y. Wang, D. Chen, and X. Zhang, “Calculated Equation of State of Al, Cu, Ta, Mo, and W to 1000 GPa,” *Physical Review Letters* **84**, 3220–3223 (2000).
- ¹⁵P. I. Dorogokupets, T. S. Sokolova, B. S. Danilov, and K. D. Litasov, “Near-absolute equations of state of diamond, Ag, Al, Au, Cu, Mo, Nb, Pt, Ta, and W for quasi-hydrostatic conditions,” *Geodynamics & Tectonophysics* **3**, 129–166 (2012).
- ¹⁶J. P. Perdew and Y. Wang, “Accurate and simple analytic representation of the electron-gas correlation energy,” *Physical Review B* **45**, 13244–13249 (1992).
- ¹⁷T. S. Sokolova, P. I. Dorogokupets, and K. D. Litasov, “Self-consistent pressure scales based on the equations of state for ruby, diamond, mgo, b2-nacl, as well as au, pt, and other metals to 4 mbar and 3000 k,” *Russian Geology and Geophysics* **54**, 181–199 (2013).
- ¹⁸F. C. Nix and D. MacNair, “The Thermal Expansion of Pure Metals. II: Molybdenum, Palladium, Silver, Tantalum, Tungsten, Platinum, and Lead,” *Phys. Rev.* **61**, 74–78 (1942).
- ¹⁹R. K. Kirby, T. A. Hahn, and B. D. Rothrock, *American Institute of Physics Handbook 3rd edn*, edited by F. Mandl, Vol. 4 (McGraw-Hill, New York, New York, USA, 1973).
- ²⁰A. P. Miiller and A. Cezairliyan, “Thermal expansion of molybdenum in the range 1500–2800 k by a transient interferometric technique,” *International Journal of Thermophysics* **6**, 695–704 (1985).

- ²¹V. Y. Bodryakov, “Correlation of temperature dependencies of thermal expansion and heat capacity of refractory metal up to the melting point: Molybdenum,” *High Temperature* **52**, 840–845 (2014).
- ²²A. F. Guillermet and G. Grimvall, “Analysis of thermodynamic properties of molybdenum and tungsten at high temperatures,” *Physical Review B* **44**, 4332–4340 (1991).
- ²³J. M. Dickinson and P. E. Armstrong, “Temperature dependence of the elastic constants of molybdenum,” *Journal of Applied Physics* **38**, 602–606 (1967).
- ²⁴D. I. Bolef and J. de Klerk, “Elastic Constants of Single-Crystal Mo and W between 77° and 500°K,” *Journal of Applied Physics* **33**, 2311–2314 (1962).
- ²⁵P. Bujard, R. Sanjines, E. Walker, J. Ashkenazi, and M. Peter, “Elastic constants in nb-mo alloys from zero temperature to the melting point: experiment and theory,” *Journal of Physics F: Metal Physics* **11**, 775–786 (1981).